Photophysics of Xanthone: A Quantum Chemical Perusal

ARTICLE *in* THE JOURNAL OF PHYSICAL CHEMISTRY A · MAY 2013

Impact Factor: 2.69 · DOI: 10.1021/jp401755j · Source: PubMed

3 AUTHORS, INCLUDING:

Vidisha Rai-Constapel
Heinrich-Heine-Universität Düsseldorf
16 PUBLICATIONS **64** CITATIONS

THE JOURNAL OF PHYSICAL CHEMISTRY A

Article

pubs.acs.org/JPCA

Photophysics of Xanthone: A Quantum Chemical Perusal

Vidisha Rai-Constapel,*[,†] Mihajlo Etinski,[†,‡] and Christel M. Marian[†]

[†]Institute of Theoretical and Computational Chemistry, Heinrich Heine University Düsseldorf, Universitätsstrasse 1, D-40225 Düsseldorf, Germany

[‡]Faculty of Physical Chemistry, University of Belgrade, Studentski trg 12-16, 11158 Belgrade, Serbia

ABSTRACT: A theoretical analysis of the chromophore xanthone has been carried out in various cases, starting from the isolated molecule and going on to the extremely polar-protic solvated chromophore. In the gas phase, we find that an El-Sayed forbidden channel with a rate constant of $k_{ISC} = 2 \times 10^{11}$ s^{-1} is one of the trend-setting factors in the photophysical kinetics. The fluorescence is found to be quenched in the gas phase and polar-aprotic solvents. The analysis of xanthone in aqueous solution supports the delayed fluorescence model, which has been suggested to explain the high fluorescence quantum yield observed in water. Besides, we present a detailed analysis of the photophysics of xanthone in acetonitrile and methanol.

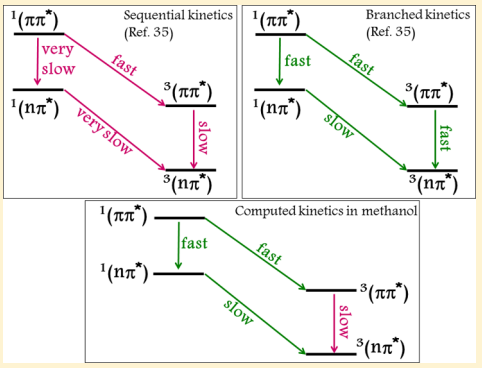

1. INTRODUCTION

The xanthone group of aromatic ketones, thioxanthone (Figure 1 with X = S), xanthone (Figure 1 with X = O), and acridone

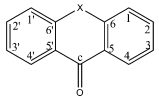

Figure 1. Chemical structure and labeling of xanthones (X = S, O, NH).

(Figure 1 with X = NH), along with their derivatives, are a well-known group of triplet sensitizers finding application, for example, as initiators of photopolymerization.[1] Their pharmaceutical properties,[2−5] such as anticarcinogenic, antibacterial, anti-inflammatory, make them a subject of intense medicinal research. In our two previous papers,[6,7] we have presented a detailed discussion of thioxanthone (TX). We focus our attention on xanthone (X) in the present work with emphasis on the solvatochromicity and various aspects of photophysical relaxation processes.

In all of the applications of these chromophores, the excited-state energetics plays an important role. A good triplet sensitizer should command over triplet states, which are populated via fast ISC from a close-lying photoexcited singlet state. The energetic layout of the excited states is, hence, of major interest. With the help of various spectroscopical methods, experimentalists can very accurately determine the energetic position of the optically bright singlet and triplet states. However, the dark states are literally in the dark as far as experimental observations are concerned. The fact that these dark states play a major role in the photophysics is well accepted. An illustrating example was the case of thioxanthone in methanol.[7] In this case, the vicinity of the $T(n_O\pi^*_L)$ and $S(\pi_H\pi^*_L)$ provided for an explanation with regard to the delayed fluorescence observed.[8] Our computational technique played an important role towards the verification of this observation by providing a very good description of the character and adiabatic minima of the low-lying excited states of TX in methanol.

As triplet sensitizers, these groups of molecules should show a high triplet quantum yield. Usually a triplet state would be populated via intersystem crossing (ISC) with a suitable singlet state. Hence, it is important to understand

- the character of the lowest-lying triplet state,
- the character of the singlet states in the vicinity of the triplet state of interest,
- and the various radiative or radiationless channels available at the singlet state minimum to which photoexcitation occurs.

The spectroscopic behavior of X in various solvents has been the subject of a lot of discussion. In particular, the route populating its lowest triplet state is of major interest. Connors and Christian studied the phosphoresence spectrum of X.[9] An analysis of the temperature dependence of such a spectrum caused these authors to assign $(\pi\pi^*)$ character to the lowest triplet state of X in apolar solvents, as opposed to the assignment earlier offered by Pownall and Hubner.[10] The former authors based their interpretation of the temperature dependence on the blue shift of $(n\pi^*)$ states in polar solvents causing a larger triplet−triplet energy gap. According to these authors, the lowest triplet state retains the $(\pi\pi^*)$ character, irrespective of the solvent. The authors Pownall and Hubner,[10] however, base their explanation of this phenomenon on a crossing of the lowest-lying triplet $(n\pi^*)$ and $(\pi\pi^*)$ states. According to them,

Received: February 19, 2013
Revised: April 14, 2013
Published: April 16, 2013

in apolar solvents the lowest triplet state has (nπ^*) character, whereas this changes to ($\pi\pi^*$) character as one goes to polar solvents. It is, meanwhile, well accepted that the lowest triplet and singlet states of X in apolar medium have (nπ^*) character and that this changes with respect to the polarity and proticity of the solvent. However, the extent of the solvatochromatic shifts is not clear. For example, it has been said that the destabilization of the (nπ^*) states in polar solvents is comparatively less than the stabilization that the ($\pi\pi^*$) states experience.[11−13] In section 3.1, we shall present a detailed quantitative discussion of the effect of solvation on the vertical excitation spectrum.

Cavaleri et al.[12] observed a biphasic rise of the triplet absorption spectrum. According to them, the dynamics can be explained by taking into account that the absorbing triplet state is populated via two different pathways. They propose two El-Sayed allowed processes leading to such a biphasic rise: (a) direct ISC from $^1(\pi\pi^*) \rightsquigarrow {}^3(n\pi^*)$ followed by IC to the $^3(\pi\pi^*)$ state; and (b) fast IC from $^1(\pi\pi^*)$ to $^1(n\pi^*)$, which is followed by ISC to the $^3(\pi\pi^*)$ state. This scheme is mentioned as the branched kinetics by Satzger et al. (see Figure 2 in ref 11).

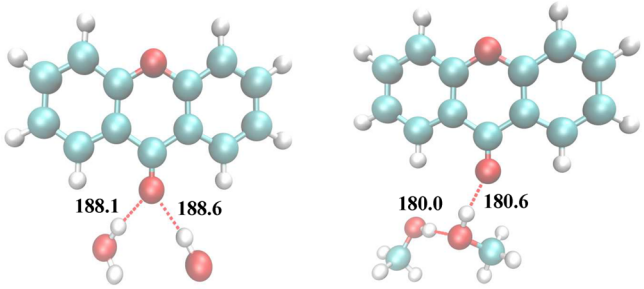

Figure 2. Solvent model for X.

These latter authors propose the sequential kinetics as the more likely mechanism. According to this, the IC between the involved singlet states is too weak as compared to the very fast ISC process $^1(\pi\pi) \rightsquigarrow {}^3(n\pi^*)$. This is then followed by a slower IC to the absorbing $^3(\pi\pi^*)$ state. Section 3.3 deals with this topic from a computational point of view.

2. METHODS AND COMPUTATIONAL DETAILS

The technical details of the basis sets, functionals, and methods used for geometry optimization of the ground and excited states of X can be found in a previous work.[6] As in the case of TX, the calculations for the ground and excited states were performed in C_{2v} symmetry. To test if the resulting geometries correspond to true minima of the potential energy hypersurface (PEH), harmonic vibrational frequencies were calculated numerically with the program SNF.[14]

To mimic the solvent environment in theoretical calculations, conductor-like screening model (COSMO) has proven to be very reliable.[15−17] The continuum model COSMO implemented in the Turbomole package[18,19] has been utilized in the present work to study X in acetonitrile, MeOH, and H_2O. As has already been discussed in the previous work,[7] in the case of MeOH and H_2O one has to take the specific bonding between the solvent and chromophore into account. To do this, we took our best model of X with two MeOH and H_2O molecules in the vicinity of the carbonyl oxygen (Figure 2).

Vertical electronic excitation energies, dipole (transition) moments, and oscillator strengths were obtained from subsequent single-point calculations using the combined density functional theory/multireference configuration interaction (DFT/MRCI) method of Grimme and Waletzke.[20] This approach represents an effective means to obtain spin-restricted electronic spectra for organic systems with errors typically less than 0.2 eV.[20−22] The 1s electrons of carbon, oxygen, and nitrogen constitute a frozen core, and the valence electrons were correlated. In addition to the $^1A_1$ ground state, five excited states were calculated in all of the irreducible representations (IRs) of C_{2v} symmetry for both singlet and triplet manifolds. Because of technical reasons, C_1 symmetry had to be used for all calculations involving COSMO and DFT/MRCI.

To qualitatively understand the photophysical processes that a photoexcited chromophore may undergo, we determine the linearly interpolated path (LIP) between the minima of involved states using the program package DISTORT.[23] A single-point DFT/MRCI calculation is carried out at each displacement to determine the vertical excitation energy profile of the singlet and triplet manifolds.

Computation of the ISC rate requires the electronic spin−orbit coupling matrix element. Spin−orbit matrix elements (SOMEs) between the correlated DFT/MRCI wave functions have been determined using the SPOCK program developed in our laboratory.[24,25] The vibrational frequencies determined by the program SNF are used as input to compute the rate constants. The ISC rates have been calculated perturbationally according to the Golden rule approximation using the VIBES program. In the case of decay of an initially populated singlet vibronic state $|S_a,\nu_{aj}\rangle$ to a quasicontinuum of final vibronic states $|T_b^\alpha,\{\nu_{bk}\}\rangle$ belonging to the α-component of a triplet electronic state, the rate is given:

$$k_{\mathrm{ISC}} = 2\pi \sum_k |\langle S_a, \nu_{aj}|\hat{\mathcal{H}}_{\mathrm{SO}}|T_b^\alpha, \nu_{bk}\rangle|^2 \delta(E_{aj} - E_{bk}) \quad (1)$$

and in the case of a decay from a manifold of thermally populated vibronic states, the rate is given:

$$k_{\mathrm{ISC}} = \frac{2\pi}{Z} \sum_{j,k} \mathrm{e}^{-\beta E_j} |\langle S_a, \nu_{aj}|\hat{\mathcal{H}}_{\mathrm{SO}}|T_b^\alpha, \nu_{bk}\rangle|^2 \delta(E_{aj} - E_{bk}) \quad (2)$$

where Z is a canonical partition function for vibrational motion in the singlet electronic state, E_{aj} and E_{bk} are the energies of initial and final vibronic states, and E_j is the vibrational energy of the initial vibronic state.

If the SOMEs are small as is the case between the electronic states with the same orbital momentum, it is necessary to take into account its dependence on the nuclear coordinates:

$$\langle S_a, \nu_{aj}|\hat{\mathcal{H}}_{\mathrm{SO}}|T_b^\alpha, \nu_{bk}\rangle = \langle \nu_{aj}|\langle S_a, |\hat{\mathcal{H}}_{\mathrm{SO}}|T_b^\alpha\rangle|_{q_0}|\nu_{bk}\rangle \quad (3)$$

$$+ \langle \nu_{aj}| \sum_m \left.\frac{\partial\langle S_a|\hat{\mathcal{H}}_{\mathrm{SO}}|T_b^\alpha\rangle}{\partial Q_m}\right|_{q_0} Q_m \nu_{bk}\rangle \quad (4)$$

$$+ \ldots$$

where Q_m are normal modes of the initial electronic state, and the expansion is taken around the equilibrium geometry of initial electronic state. The zero-order term in the Taylor expansion of SOMEs contributes to direct spin−orbit coupling, while the term linear in the nuclear coordinates contributes to vibronic spin−orbit coupling.[26] The direct spin−orbit coupling is equivalent to the Condon approximation for SOMEs; hence the calculation of ISC rate is reduced to evaluation of electronic SOMEs

dx.doi.org/10.1021/jp401755j | J. Phys. Chem. A 2013, 117, 3935−3944

Table 1. Selected Ground- and Excited-State Geometries Bond Lengths (pm) and Bond Angles (deg) of X[a]

	DFT C_{2v} structure					S_0 structure[b]		
	S_0[b]	$S_1(n_O\pi^*)$[c]	$S_2(\pi\pi^*)$[c]	$T_1(n_O\pi^*)$[c]	$T_2(\pi\pi^*)$[c]	acetonitrile	methanol	water
$r(C_1-C_2)$	138.2	139.6	140.5	139.5	139.3	138.3	138.3	138.2
$r(C_2-C_3)$	140.0	139.6	138.7	139.5	140.5	140.3	140.3	140.3
$r(C_3-C_4)$	138.0	138.4	141.4	138.5	137.9	138.1	138.0	138.0
$r(C_4-C_5)$	140.2	141.7	139.4	141.3	141.7	140.5	140.6	140.8
$r(C_5-C_6)$	139.8	141.6	141.3	141.4	142.8	140.1	140.1	140.3
$r(C_6-C_1)$	139.5	138.2	139.4	138.3	138.2	139.6	139.6	139.6
$r(C_6-O)$	136.5	136.9	136.6	137.2	137.2	136.6	136.4	136.2
$r(C_5-C_c)$	147.5	142.2	146.6	142.5	142.8	147.0	146.6	146.2
$r(C_c-O)$	122.2	131.5	124.7	132.0	135.6	123.2	123.7	124.3
$\angle(C_6OC_6')$	119.8	121.0	121.4	121.0	122.0	119.9	120.0	120.0
$\angle(C_5C_cC_5')$	114.3	120.0	114.5	121.0	120.0	114.8	115.3	115.6
$\angle(C_6C_5OC_6')$	180.0	180.0	179.5	180.0	180.0	179.9	179.6	179.6

[a]Atomic labels are displayed in Figure 1. [b]DFT/B3LYP/TZVP results. [c]TDDFT/B3LYP/TZVP results.

Table 2. Vertical Singlet and Triplet Excitation Energies ΔE (eV) at the Ground-State Minimum of Xanthone in Vacuum and Solvents

state		electronic structure	ΔE vacuum	AcN	MeOH	water	literature
S_0	1^1A_1	(94.7) ground state	0.00	0.00	0.00	0.00	
S_1	1^1A_2	(75.4) $n_O \rightarrow \pi_L^*$	3.44	3.67	3.79	4.03	3.34,[a] 3.43,[b] 3.44[c]
S_2	2^1A_1	(75.7) $\pi_H \rightarrow \pi_L^*$	3.88	3.80	3.74	3.67	3.81,[a] 3.65,[b] 3.69[c]
T_1	1^3A_2	(76.8) $n_O \rightarrow \pi_L^*$	3.26	3.51	3.64	3.88	3.20,[a] 3.15,[b] 3.22[c]
T_2	1^3A_1	(66.4) $\pi_H \rightarrow \pi_L^*$, (15.2) $\pi_{H-2} \rightarrow \pi_L^*$	3.32	3.26	3.20	3.13	3.21[b]
T_3	2^3A_1	(47.3) $\pi_{H-2} \rightarrow \pi_L^*$, (15.9) $\pi_H \rightarrow \pi_L^*$, (11.6) $\pi_{H-3} \rightarrow \pi_{L+2}^*$	3.58	3.39	3.56	3.56	
T_4	1^3B_2	(42.9) $\pi_{H-1} \rightarrow \pi_L^*$, (13.2) $\pi_{H-2} \rightarrow \pi_{L+2}^*$	3.66	3.39	3.60	3.56	

[a]Jet-cooled xanthone.[30] [b]Xanthone in hexane.[12] [c]Reference 28.

and normal mode wave function overlap integrals. The ISC rate using the vibronic spin−orbit coupling is obtained by calculating the derivative of the electronic SOMEs with respect to the normal coordinates and integrals involving a product of normal mode coordinates and their wave functions.

To obtain the ISC rate using direct and vibronic spin−orbit coupling, we employed two methods. The first method, called time-independent, is based on the direct evaluation of normal mode wave function integrals in a selected energy interval around the initial state.[27] The second method, called time-dependent, calculates the ISC rate as an integral of the time correlation function.

3. RESULTS AND DISCUSSION

3.1. Vertical Excitation Spectra: Vacuum and Solvent.

Table 1 lists the geometrical parameters for the ground and the lowest-lying singlet and triplet states of X optimized during this work. Onuma and Ijima[28] studied the molecular structure of X in gas and solid phases. A planar strucutre was assigned by them to X in the gas phase. They assumed the benzene ring structure to be a regular hexagon; however, the symmetry of the ring was found to be lower. This can be verified by our calculations, which show that the benzene rings are not regular hexagons (see Table 1). Another crystallographic structure study of X also supports the planar ground-state conformation.[29]

The benzene ring structure in solvent environment is hardly deformed as compared to the vacuum ground-state equilibrium (see Table 1). The most noticeable change is the slight stretching of the C_c-O bond. In the case of X, this varied from 1 pm (in acetonitrile), over 1.5 pm (in MeOH), to 2.1 pm (in H_2O). The electron density distribution on the chromophore is not deformed after solvation, a fact that is underlined by these minimal structural variations after the solvation process.

Table 2 lists the vertical DFT/MRCI excitation energies at the electronic ground-state equilibrium for X in vacuum and various solvents. The calculations performed for an isolated chromophore, that is, in vacuum can be compared to experiments carried out in the gas phase or apolar solvents. In the case of TX,[6] the respective energetic position of the lowest-lying $^1(n_O\pi_L^*)$ and $^1(\pi_H\pi_L^*)$ excited states in the vertical excitation spectrum was a topic of discussion, because this would affect the photophysics of the species. The reason was the near degeneracy of the two states (ΔE = 0.07 eV) . In the case of X, there can be no such confusion as the two states are energetically well separated (Table 2, ΔE = 0.44 eV). Ohshima et al.[30] have studied the two lowest-lying singlet states of jet-cooled X. They assign the 0_0^0 band at 3.34 eV to the $S_0 \rightarrow S_1(n_O\pi_H^*)$ transition. This is in perfect agreement with our calculated spectrum (see Table 2).

The energetic position of the triplet states is of central interest in this group of molecules, as they are used largely as triplet sensitizers. There are four triplets to be found below the optically active $S_2(\pi_H\pi_L^*)$ state. The first triplet is determined to have $(n_O\pi_L^*)$ character. Ishijima et al.[31] analyzed the MCD spectrum of X in *n*-pentane and compared it to the spectrum in 1-iodopentane and came to the same conclusion. Besides, the quantitative agreement in the energetic whereabout of this state is also in perfect agreement (see Table 2). The excitation energy of 3.20 eV reported by Ohshima[30] shows complete agreement with the excitation energy of 3.26 eV reported in this

dx.doi.org/10.1021/jp401755j | J. Phys. Chem. A 2013, 117, 3935−3944

work. The character of the lowest-lying triplet state is an important issue as the radiationless and radiative relaxation channels to the ground state would depend on whether the ($n\pi^*$) or the ($\pi\pi^*$) character is dominating (see Ssection 3.3).

As is to be expected, the ($\pi\pi^*$) states are red-shifted as the polarity of the solvent increases, whereas the ($n\pi^*$) states are pushed to higher energies due to solvation. The blue shift experienced by the ($n\pi^*$) states is comparatively large, being ~0.24 eV in acetonitrile, ~0.35 eV in MeOH, and peaking to ~0.60 eV in H_2O. In comparison, the red shift experienced by the various ($\pi\pi^*$) states is less than one-half this amount and in some cases even an order of magnitude smaller (Figure 3). This

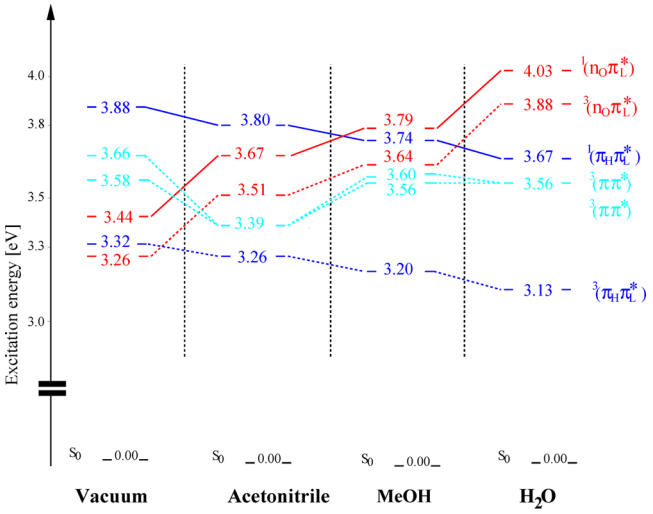

Figure 3. Comparison of the vertical excitation energies in vacuum, acetonitrile, methanol, and water for X.

finding refutes the previous assumption indicating that the red shift is much larger as compared to the blue shift.[13] The polarities of acetonitrile and MeOH are quite similar. The batho- and hypsochromic shifts are, however, in the two cases quite different due to the proticity of MeOH.

3.2. The Adiabatic Minima in Vacuum. It is quite obvious that the adiabatic minima of the excited states have to be investigated to understand the photophysical processes a species may undergo after photoexcitation.

3.2.1. ($n_O\pi_L^*$) States: The True Minimum? Because of the spin selection rule, photoexcitation from the singlet ground state in the current molecules would occur to the next available singlet state. However, this is not the only criterium. The photoexcitation would only take place to a $^1(\pi_H\pi_L^*)$ excited state. These states are the so-called bright states. If a state of ($n_O\pi_L^*$) character lies energetically below, it would usually not be seen in a conventional spectrum due to small transition dipole moment and is, hence, named the dark state. In our previous paper, we have been able to establish that the true minimum of the first singlet excited state in TX has ($n_O\pi_L^*$) character in the gas phase.[7] This fact was seen to be of great importance for the radiative and radiationless processes occurring after photoexcitation.

As was already mentioned in section 3.1, the lowest excited singlet of X in vacuum is found to be a dark ($^1n_O\pi_L^*$) state with a planar C_{2v} symmetric minimum. The vertical excitation spectrum (see Table 2) reveals that the lowest state in the triplet manifold also has a ($n_O\pi_L^*$) character. The TDDFT(B3LYP) optimized C_{2v} structure of this state turns out to be a first-order saddle point. One imaginary frequency is obtained ($\bar{\nu}_1 = i321$ cm^{-1}) for an A_2-symmetric normal mode, which corresponds to an asymmetrical butterfly mode. An optimization carried out at the lowered symmetry brings to light the degeneracy of the $^3(\pi_H\pi_L^*)$ and $^3(n_O\pi_L^*)$ states at the adiabatic minimum of the $^3(n_O\pi_L^*)$ electronic state. TDDFT then fails to carry out an optimization of the required state. To compute the ISC rates involving this state, we have used the normal-mode frequencies of the corresponding singlet state. The parallel course of the potential curves of these two states (see Figure 4) supplies countenance to this procedure.

For the purpose of better understanding the geometrical variations upon excitation, the involved frontier orbitals are depicted in Figure 5. The most striking structural change upon $n_O \rightarrow \pi_L^*$ excitation is the stretching of the C_c–O bond by 9–10 pm (see Table 1). The C_c–C_5 bond is shortened by about 5 pm. The nonbonding character of the lone-pair oxygen orbital changes to antibonding with respect to the C_c–O bond upon $n_O \rightarrow \pi_L^*$ excitation, resulting in a large stretching of this bond. Similarly, the antibonding character of the C_c–C_5 bond is changed to bonding leading to shorter bond lengths. This is true for both the singlet and the triplet electronic state arising from this excitation.

The adiabatic excitation energy of the singlet state is 3.08 eV (see Table 3). The adiabatic minimum of the state is stabilized by 0.35 eV with respect to the vertical absorption region. The ground-state destabilization being 0.39 eV, the vertical emission energy can be determined as 2.69 eV. On symmetry grounds, a radiative decay to the ground state is not dipole-allowed. The corresponding triplet state is stabilized by 0.46 eV.

Adiabatic excitation energies of excited electronic states have been estimated (ΔE_{est} in Table 3) in various solvents via application of the appropriate solvent shifts, experienced by the individual states at the Franck–Condon point in vacuum, to the adiabatic energies of the respective states determined in vacuum. The $^1(n_O\pi_L^*)$ state is clearly the first excited singlet state in the gas phase, and this remains true for acetonitrile and MeOH solvent environments. On the other hand, the corresponding triplet is the lowest excited state in the triplet manifold only for vacuum.

3.2.2. ($\pi_H\pi_L^*$) States. Because the photoexcitation is to the first optically bright singlet state, we discuss here in detail the adiabatic minimum of the $^1(\pi_H\pi_L^*)$ state. The optimized structural parameters are listed in Table 1.

The first optically bright transition is the $\pi_H \rightarrow \pi_L^*$ excitation. From the electron density distribution at the involved orbitals (see Figure 5), one can draw some conclusions as to how the geometry of the resulting singlet and triplet states would vary in comparison to that of the ground state. As compared to the ($n_O\pi_L^*$) states, the geometrical variations are moderate. The most noticeable change occurs at the C_c–O and C_6–C_5 bonds. The antibonding character of the C_c–O bond increases in π_L^* as compared to π_H, and, hence, this bond length is stretched by about 2.5 pm. A decrease in the bonding character of C_6–C_5 (C_6'–C_5') bond causes this to lengthen by about 1 pm. In a similar fashion, the other variations in the structure of the $^1(\pi_H\pi_L^*)$ state may be understood.

The triplet state arising from the $\pi_H \rightarrow \pi_L^*$ excitation is expected to have nearly the same structure. However, this does not seem to be the case. In particular, the C_c–O and C_5–C_c (C_5'–C_c) bonds show a much larger variation than the corresponding singlet state. In the triplet state, the C_c–O

dx.doi.org/10.1021/jp401755j | J. Phys. Chem. A 2013, 117, 3935–3944

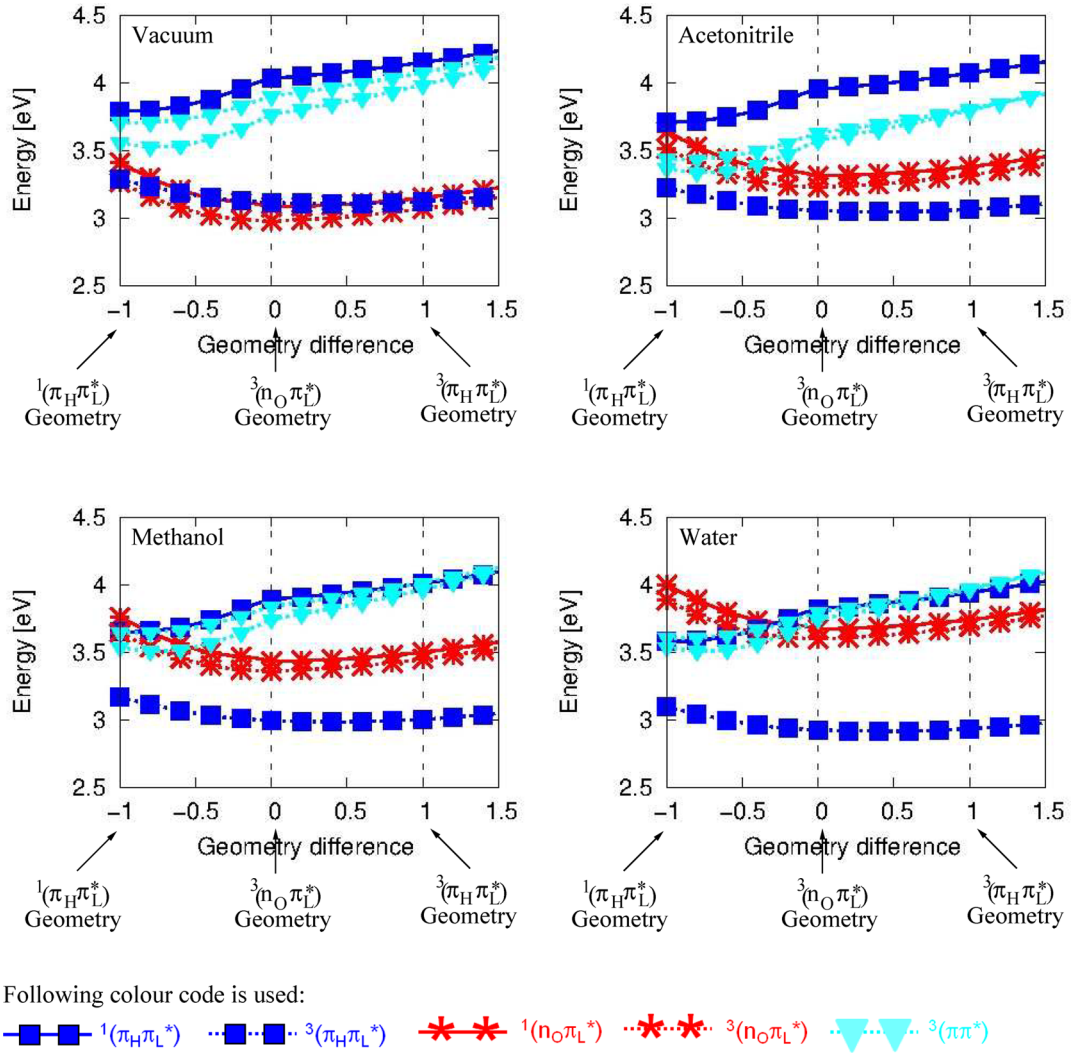

Figure 4. DFT/MRCI excitation energy profiles along a linearly interpolated path between the $^1(\pi_H\pi_L^*)$ and $^3(\pi_H\pi_L^*)$ minimum geometries of X in various cases.

bond is stretched by 13.4 pm, about 6 times that in the corresponding singlet. This anomaly is due to the additional 15% contribution of the $\pi_{H-2} \rightarrow \pi_L^*$ excitation. The antibonding character of the C_c-O bond is enhanced due to this contribution. At the same time, the C_5-C_c ($C_5'-C_c$) bond shows an increased bonding character leading to further shortening of this bond length. Analogous behavior was also found in TX.[7]

The optimized geometry of the singlet state is stabilized by 0.09 eV relative to the vertical excitation at the Franck–Condon point. The ground-state destabilization is 0.17 eV at this minimum, resulting in a vertical emission energy of 3.62 eV. The corresponding triplet state has an adiabatic excitation energy of 3.12 eV (Table 3).

3.2.3. Further $^3(\pi\pi^*)$ States. There are two multiconfigurational $^3(\pi\pi_L^*)$ states in the vertical excitation spectrum of X (Table 2), which lie below the optically bright state in vacuum. The frequency analysis of T_3 state at C_{2v} PEH possesses an imaginary frequency $\bar{\nu}_1 = i1835$ cm^{-1} corresponding to an in-plane B_2 mode. The T_4 state has a planar C_{2v} symmetric minimum.

3.3. Intersystem Crossing. The rates of nonradiative transition from the initially photoexcited singlet state to a final electronic state of either equal multiplicity (internal conversion) or different multiplicity (intersystem crossing) depend on various factors, that is, the size of the electronic coupling, the overlap of the initial and final vibrational wave functions, as well as the density of vibrational states in the potential well of the accepting state. With regard to the electronic coupling strength, it is well-known[32] that SOMEs of heteroaromatic molecules can adopt sizable values if the transition is accompanied by a change of orbital character. This is, for instance, the case for $(n\pi^*) \rightsquigarrow (\pi\pi^*)$ transitions and vice versa. $^1(\pi\pi^*) \rightsquigarrow {}^3(\pi\pi^*)$ transitions may gain intensity through vibronic coupling to a closeby $(n\pi^*)$ state though.[16,17,27,33] The contributions of the nuclear wave functions to the transition probability are to a large extent ruled by the gap between the adiabatic energies of the states involved and by the coordinate displacements of their minimum nuclear arrangements.[34] In the weak coupling case, that is, for small nuclear displacements, the energy gap is the decisive quantity. In contrast, in the strong coupling case, that is, for large displacements, an inverted region exists in which the transition moment increases with increasing energy gap before the regular exponential decrease of the rate sets in. Figure 4 shows the PES trails of the electronic states of interest in vacuum and various media. The striking features are the parallel tracks of the triplet $(n_O\pi_L^*)$ and $(\pi_H\pi_L^*)$

dx.doi.org/10.1021/jp401755j | J. Phys. Chem. A 2013, 117, 3935–3944

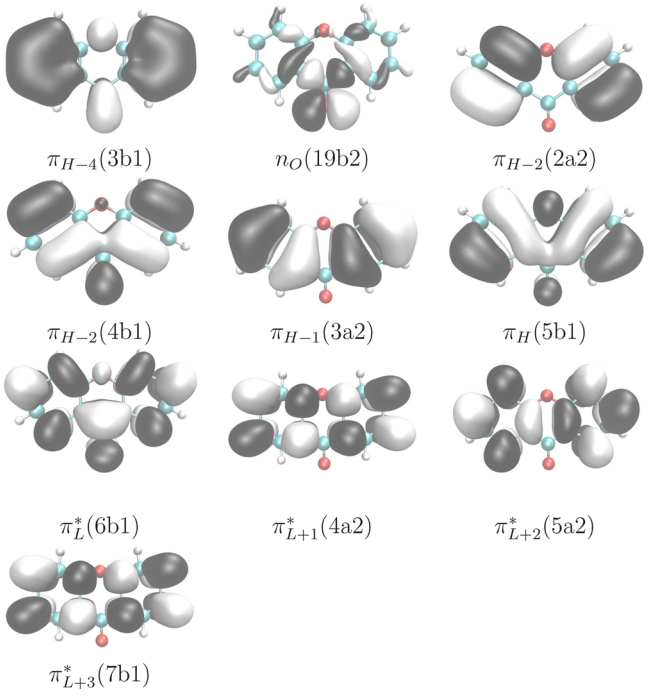

Figure 5. Frontier orbitals at the optimized ground-state (S_0) geometry (isovalue = 0.02).

states and the nonparallel tracks of the corresponding singlet states. The parallel run of the triplet PESs indicates a weak coupling case as defined by Englman and Jortner.[34] The IC rate between these two states should decrease exponentially with increasing energy difference. In the case of the corresponding singlets, however, we may expect an opposite trend because this is a strong coupling case. Throughout this work, the influence of the solvent on the molecular geometry is computed to be small (section 3.1). Environment effects are therefore expected to be mainly caused by differential energetic shifts of the electronic states due to interaction with the solvent.

For intersystem crossing to be efficient, it has to compete not only with internal conversion but also with radiative decay channels. Typical fluorescence rates are of the order of 10^9 s^{-1} for $^1(\pi\pi^*)$ emission and 2 orders of magnitude smaller for $^1(n\pi^*)$ transitions. In the following, we discuss these channels in detail for the isolated and solvated molecule.

3.3.1. Vacuum. Cavaleri et al.[12] discuss the biexponential growth of triplet−triplet absorption in various solvents. Their results for hexane are best suited for comparsion purposes with our vacuum results. According to these authors, this biphasic behavior is explained on the basis of allowed El-Sayed ISC where the $^1(\pi_H\pi^*_L) \rightsquigarrow {}^3(n_O\pi^*_L)$ channel is determined to have a time constant of about 0.70 ps and the later rise is contributed to the $^1(n_O\pi^*_L) \rightsquigarrow {}^3(\pi_H\pi^*_L)$ channel with a time constant of 10.0 ps approximately. With our computational tools, we have been able to gain a better understanding of the kinetics leading to this biphasic rise. In the following, we present our interpretation.

An at a glance visualization of the various relaxation channels is given via the LIP (Figure 4) commencing at the adiabatic minimum of the optically bright $^1(\pi_H\pi^*_L)$ state for various cases. According to our calculations, four triplet states are located adiabatically below the minimum of the initially populated $^1(\pi_H\pi^*_L)$ state in isolated X (Table 3). In addition, the minimum of the $^1(n_O\pi^*_L)$ state is found well below that of the $^1(\pi_H\pi^*_L)$ state. The $^3(n_O\pi^*_L)$ state is the lowest excited state in vacuum, lying adiabatically 0.10 eV below its singlet counterpart, while the $^1(n_O\pi^*_L)$ and $^3(\pi_H\pi^*_L)$ minima are near degenerate. A rate constant of $k_{ISC} = 5 \times 10^9$ s^{-1} (see Table 4) is calculated for the ISC channel connecting the lowest vibrational level of the $^1(\pi_H\pi^*_L)$ state and higher vibrational levels of the $^3(n_O\pi^*_L)$ state.

The close proximity of the triplet $(\pi_H\pi^*_L)$ and $(n_O\pi^*_L)$ states in vacuum (ΔE^{ad} = 0.14 eV), and the large SOME between the $^1(n_O\pi^*_L)$ and $^3(\pi_H\pi^*_L)$ states (Table 4), allow us to conclude that even El-Sayed forbidden ISC processes have to be considered (Figure 6). Although it may seem that the $^3(\pi_H\pi^*_L)$ state is not accessible from the $^1(n_O\pi^*_L)$ levels (ΔE^{ad} = −0.04 eV), the rate computed at room temperature shows this channel to be a thermally activated ultrafast process with a rate constant $k_{ISC} = 7.4 \times 10^{12}$ s^{-1}. Besides, the $^3(\pi_H\pi^*_L)$ state could mediate vibronic spin−orbit coupling between the $^1(n_O\pi^*_L)$ and $^3(n_O\pi^*_L)$ states, or may itself couple vibronically with the corresponding $^1(\pi_H\pi^*_L)$ state. The ISC rates for the two vibronic channels are computed as 3×10^9 s^{-1} (between $n_O\pi^*_L$ states) and 2×10^{11} s^{-1} (between $\pi_H\pi^*_L$ states, see Table 4 and Figure 6), respectively. As expected, the most important mode involved in the $^1(\pi_H\pi^*_L) \rightsquigarrow {}^3(\pi_H\pi^*_L)$ vibronic coupling is the C═O stretch mode, with the derivative of the SOME being −25.91 cm^{-1}. In the case of $n_O\pi^*_L$ states, it is the asymmetric out-of-plane mode (366.3 cm^{-1}) that distorts the central ring containing the two oxygen atoms (SOME derivative being 16.72 cm^{-1}), which couples the two states.

The time constants of 10.0 and 0.70 ps reported by Cavaleri et al.[12] for the direct ISC channels in hexane are in very good agreement with our rate constants for the vibronic $^1(\pi_H\pi^*_L) \rightsquigarrow {}^3(\pi_H\pi^*_L)$ channel and the direct ISC $^1(n_O\pi^*_L) \rightsquigarrow {}^3(\pi_H\pi^*_L)$, respectively (Figure 6). The time constant of 0.70 ps assigned in ref 11 to the $^1(\pi_H\pi^*_L) \rightsquigarrow {}^3(n_O\pi^*_L)$ channel indicates a fast decay in the population of the $^1(\pi_H\pi^*_L)$ state. That the ISC from this state

Table 3. Adiabatic Singlet and Triplet DFT/MRCI Excitation Energies ΔE_{adia} (eV) and Zero-Point Vibrational Energy Corrections (ZPVE) (eV) of Low-Lying Excited States of X

	vacuum		acetonitrile		MeOH		water	
geometry	ΔE_{adia}	ZPVE	ΔE_{adia}	ΔE_{est}	ΔE_{adia}	ΔE_{est}	ΔE_{adia}	ΔE_{est}
$^1(n_O\pi^*_L)$	3.08	−0.12	3.48	3.31		3.43		3.67
$^1(\pi_H\pi^*_L)$	3.79	−0.19	3.80	3.70	3.74	3.64		3.57
$^3(n_O\pi^*_L)$	2.98	−0.14	3.36	3.23		3.36		3.60
$^3(\pi_H\pi^*_L)$	3.12	−0.17	3.15	3.06	3.11	3.00	3.03	2.93
$^3(\pi\pi^*)^a$	3.43	−0.15		3.23		3.41		3.41
$^3(\pi\pi^*)^a$	3.55	−0.14		3.28		3.49		3.45

[a]Multiconfigurational triplet states, see Table 2.

dx.doi.org/10.1021/jp401755j | J. Phys. Chem. A 2013, 117, 3935−3944

Table 4. Calculated SOMEs (cm^{-1}), Rate Constants k_{ISC} (s^{-1}) for (S ⇝ T) ISC Channels (Left) in X and the Adiabatic Electronic Energy Difference ΔE^{ad} [eV] in Various Cases

	vacuum			acetonitrile			methanol			water		
channel i ⇝ f	SOME	ΔE^{ad}	k_{ISC}	SOME	ΔE^{ad}	k_{ISC}	SOME	ΔE^{ad}	k_{ISC}	SOME	ΔE^{ad}	k_{ISC}
					$^1(\pi_H\pi_L^*)$ Geometry							
$^1(\pi_H\pi_L^*)$ ⇝ $^3(n_O\pi_L^*)_x$		−0.80			−0.47			−0.28			+0.03	
$^1(\pi_H\pi_L^*)$ ⇝ $^3(n_O\pi_L^*)_y$		−0.80			−0.47			−0.28			+0.03	
$^1(\pi_H\pi_L^*)$ ⇝ $^3(n_O\pi_L^*)_z$	9.92	−0.80	5×10^9		−0.47	3.1×10^{10}		−0.28	1.7×10^{10}		+0.03	2.5×10^{8a}
$^1(\pi_H\pi_L^*)$ ⇝ $^3(\pi_H\pi_L^*)$		−0.67	2×10^{11}									
					$^1(n_O\pi_L^*)$ Geometry							
$^1(n_O\pi_L^*)$ ⇝ $^3(\pi_H\pi_L^*)_x$		+0.04			−0.25			−0.43			−0.74	
$^1(n_O\pi_L^*)$ ⇝ $^3(\pi_H\pi_L^*)_y$		+0.04			−0.25			−0.43			−0.74	
$^1(n_O\pi_L^*)$ ⇝ $^3(\pi_H\pi_L^*)_z$	51.19	+0.04	7.4×10^{12a}		−0.25	$\sim 10^{11}$		−0.43	5.4×10^9		−0.74	2.1×10^8
$^1(n_O\pi_L^*)$ ⇝ $^3(n_O\pi_L^*)$		−0.10	3×10^9									

[a]Rate computed at T = 298 K.

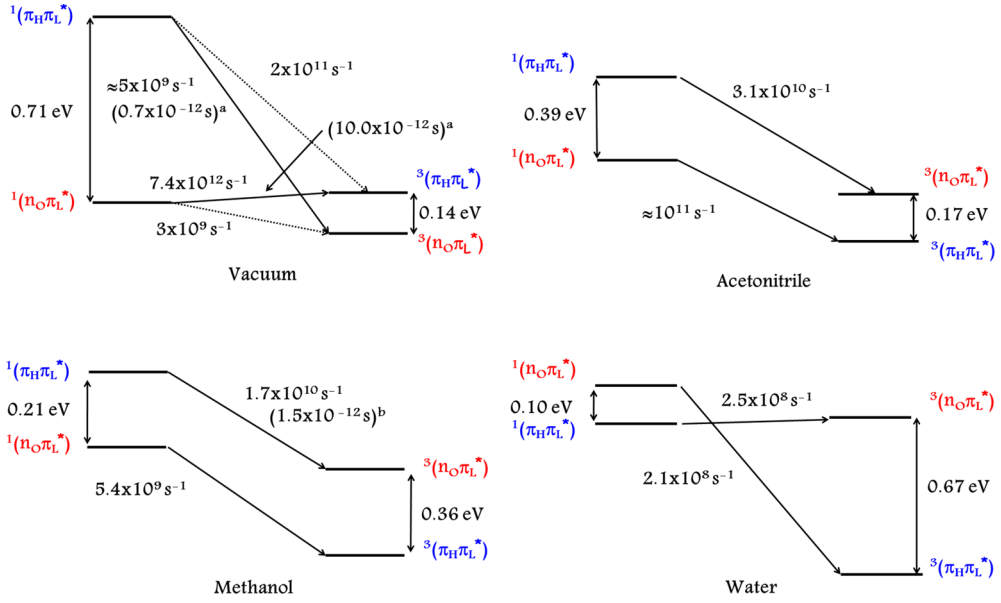

Figure 6. Qualitative picture of the various relaxation channels in vacuum and solution. The lifetimes in parentheses are the experimentally reported values. (a) Reference 12. (b) Reference 35.

takes place into the $^3(n_O\pi_L^*)$ state is taken as granted by the authors on the basis of El-Sayed rule. This may not necessarily be true, as our results show. We find that the $^1(\pi_H\pi_L^*)$ state decays via vibronic coupling to the $^3(\pi_H\pi_L^*)$ state with a rate constant that is larger by 2 orders of magnitude than that for ISC to $^3(n_O\pi_L^*)$ state (Table 4) and via IC to the lower-lying $^1(n_O\pi_L^*)$ state. The $^3(\pi_H\pi_L^*)$ state is also populated by a direct radiationless channel initiating from the $^1(n_O\pi_L^*)$ state with a large rate constant (see Table 4). The later rise in the triplet−triplet absorption is then due to IC from the $^3(\pi_H\pi_L^*)$ state. The ISC channels, $^1(\pi_H\pi_L^*)$ ⇝ $^3(n_O\pi_L^*)$ ($k_{ISC} = 5 \times 10^9$ s^{-1}) and $^1(n_O\pi_L^*)$ ⇝ $^3(n_O\pi_L^*)$ ($k_{ISC} = 3 \times 10^9$ s^{-1}), should not be very relevant as the formation of $^3(\pi_H\pi_L^*)$ state via the involved singlet states is an ultrafast process. The radiative emission from the $^1(\pi_H\pi_L^*)$ state is calculated to be slow in comparison, $k_f = 7.6 \times 10^7$ s^{-1}. Hence, fluorescence in apolar media should be quenched by radiationless channels.

As mentioned in the Introduction, the kinetics proposed by Cavaleri et al.[12] is the so-called branched kinetics. Our analysis can only partially corroborate this model for vacuum and apolar media. Branched is true in that the $^1(\pi_H\pi_L^*)$ decays via ISC to a lower-lying triplet and IC to $^1(n_O\pi_L^*)$. However, the ISC is not the usually assumed El-Sayed channel, but the vibronic $^1(\pi_H\pi_L^*)$ ⇝ $^3(\pi_H\pi_L^*)$ channel ($k_{ISC} = 2 \times 10^{11}$ s^{-1}). The step leading to the later component of the observed triplet−triplet absorption is similar to that proposed in the sequential model by Satzger et al.,[35] subsequent IC from the $^3(\pi_H\pi_L^*)$ state to the $^3(n_O\pi_L^*)$ state.

3.3.2. Solvents. When the polarity (and proticity) of the environment increases, the $(n_O\pi_L^*)$ states experience strong blue shifts with respect to the $(\pi\pi^*)$ states. As can be clearly seen from Figure 3, this variation in the energetic shift leads to a crossing between the states of interest. For the case of TX, these crossings were found to have a major impact on the photophysical behavior of the chromophore.[7] We may, hence, expect analogous photophysical adventure in X. The adiabatic energy differences between the various electronic states (see Table 3) allow us to draw some first-hand conclusions regarding the various ISC channels. The energy gap between the triplet $(n_O\pi_L^*)$ and $(\pi_H\pi_L^*)$ states increases along with the polarity and proticity of the solvent, which leads us to conclude that the vibronic coupling with the respective singlet states should lose importance in the same order. Also, the rate of IC between the two triplets would reduce as they move apart. On the other

dx.doi.org/10.1021/jp401755j | J. Phys. Chem. A 2013, 117, 3935−3944

hand, the IC between the involved singlet states should get faster because these states approach each other as one goes from vacuum to methanol. The trend reported by Cavaleri et al.[12] for this IC lends support to our analysis.

Acetonitrile. Acetonitrile is a polar aprotic solvent with relative permittivity of 36. The solvent−solute interaction is sufficient to push the $(n_O\pi_L^*)$ states well above the $^3(\pi_H\pi_L^*)$ state, the latter becoming the lowest excited electronic state in acetonitrile solution, while the $^1(n_O\pi_L^*)$ state remains the lowest excited singlet. This situation opens the possibility of several fast ISC processes: $^1(\pi_H\pi_L^*) \rightsquigarrow {}^3(n_O\pi_L^*)$ ($k_{ISC} = 3.1 \times 10^{10}$ s^{-1}) as well as $^1(n_O\pi_L^*) \rightsquigarrow {}^3(\pi_H\pi_L^*)$ ($k_{ISC} \approx 10^{11}$ s^{-1}). At the $^1(\pi_H\pi_L^*)$ minimum in acetonitrile (see Figure 4), the two singlet states are isoenergetic. Hence, we expect a very fast IC to $^1(n_O\pi_L^*)$ state, with a rate comparable to that of the ISC to $^3(n_O\pi_L^*)$ state. The proximity of the $^3(n_O\pi_L^*)$ and $^3(\pi_H\pi_L^*)$ states (see Figure 6) allows for a fast IC to the lowest triplet. The rise in the triplet absorption spectrum at later time is then due to the $^1(n_O\pi_L^*) \rightsquigarrow {}^3(\pi_H\pi_L^*)$ channel. Our analysis, thus, substantiates the branched kinetics proposed by Cavaleri et al. in polar aprotic medium like acetonitrile. Because the two triplet states are still in close vicinity to each other ($\Delta E^{ad} = 0.17$ eV), one may expect the vibronic coupling to be comparable to that in vacuum. However, the fast IC to $^1(n_O\pi_L^*)$ state would dominate over the vibronic $^1(\pi_H\pi_L^*) \rightsquigarrow {}^3(\pi_H\pi_L^*)$ channel. The $(n_O\pi_L^*)$ vibronic rate is anyway much slower than the El-Sayed allowed $^1(n_O\pi_L^*) \rightsquigarrow {}^3(\pi_H\pi_L^*)$ relaxation path. The calculated radiative rate from the $^1(\pi_H\pi_L^*)$ state is $k_f = 6.1 \times 10^7$ s^{-1}, which, being much smaller than the ISC and IC rates, indicates that fluorescence is quenched in acetonitrile.

Methanol. Methanol is comparable to acetonitrile in its polarity with a relative permittivity of 33; however, it forms hydrogen bonds with the chromophore leading to enhanced blue shift of the $(n_O\pi_L^*)$ states. This causes significant variation in the kinetics as compared to that in acetonitrile. Satzger et al.[35] have investigated the photophysics of X in ethanol. Because the two solvents, methanol and ethanol, are of comparable polarity and hydrogen-bonding capacity, we have chosen to compare our results for X in methanol to this work. In this experimental work, the authors report a time constant of 1.5 ps to describe the population transfer from the photoexcited $^1(\pi_H\pi_L^*)$ state. These authors propose the sequential kinetics in ethanol. According to this model, the biphasic rise is explained via a fast $^1(\pi_H\pi_L^*) \rightsquigarrow {}^3(n_O\pi_L^*)$ ISC (1.5 ps time constant) followed by the slower IC from $^3(n_O\pi_L^*)$ to $^3(\pi_H\pi_L^*)$ state (with 12 ps time constant). The IC from the photoexcited singlet state to the dark singlet state is said to be weak[35] as compared to the ISC to $^3(n_O\pi_L^*)$ state.

We compute the lowest excited singlet state in methanol to be the $^1(n_O\pi_L^*)$ state (Table 3). At the adiabatic minimum of the singlet $(\pi_H\pi_L^*)$ state to which the photoexcitation occurs (Figure 4), the order of the singlet states is reversed and the $^1(n_O\pi_L^*)$ state lies marginally higher in energy. One may be misled into believing that this fact would hamper the fast IC channel between the two singlet states, which is available in acetonitrile. Figure 4, however, also shows that the crossing point between the PES of the involved singlet states is quite close to the minimum of the bright singlet state; besides, the $^1(n_O\pi_L^*)$ adiabatic minimum lies well below the minimum of the former state. Hence, a fast IC between the two singlet states should be feasible and compete with the $^1(\pi_H\pi_L^*) \rightsquigarrow {}^3(n_O\pi_L^*)$ ISC relaxation channel, which has a computed rate constant of 1.7×10^{10} s^{-1}. Because of the enhanced blue shift of the $^3(n_O\pi_L^*)$ state in methanol, the energy difference between this state and the lowest-lying triplet $(\pi_H\pi_L^*)$ state is 0.36 eV, which is twice the energy difference in the acetonitrile solution (Figure 6). This being a weak coupling case (see section 3.3), a slower IC between the two triplet states is expected in methanol as compared to that in acetonitrile. The analysis above leads us to conclude that the first step after photoexcitation to $^1(\pi_H\pi_L^*)$ state obeys a branched kinetics in that both IC to $^1(n_O\pi_L^*)$ and ISC to $^3(n_O\pi_L^*)$ states should be equally possible. The second step in the biexponential rise is not that easily assigned. The two channels responsible for this are the $^1(n_O\pi_L^*) \rightsquigarrow {}^3(\pi_H\pi_L^*)$ ISC channel with a rate constant of 5.4×10^9 s^{-1} and the IC between the two triplet states. The former channel corresponds to the branched kinetics as proposed by Cavaleri et al.,[12] whereas the latter corresponds to the sequential model as proposed by Satzger et al.[35] We, hence, conclude that a combination of both models would best explain the kinetics in this case. As the energetic separation of the triplets, which could facilitate vibronic coupling, increases, we do not expect these channels to make a difference to the photophysical model as discussed above. The fluorescence rate constant is comparable to that in vacuum and acetonitrile ($k_f = 6.1 \times 10^7$ s^{-1}) and should be effectively quenched in this solvent.

Water. In water, the combined effects of polarity and hydrogen bonding are strong enough to cause a reversal of the order of singlet states with respect to vacuum conditions. In aqueous solution, fluorescence is therefore expected to be the dominant decay channel of the $^1(\pi_H\pi_L^*)$ state, in agreement with experimental observations ($\tau_{rad} \approx 20$ ns).[36] We compute a rate constant of $k_f = 6.7 \times 10^7$ s^{-1} for this radiative process, in perfect agreement with experiment.

The interesting observation for X in water was, however, the high fluorescence quantum yield. This has been explained by Heinz et al.[36] in terms of delayed fluoresence. This model is based on the idea that there exists an isoenergetic triplet state of $(n_O\pi_L^*)$ character near the bright $^1(\pi_H\pi_L^*)$ state. This allows for a back population of the singlet state after ISC into the $^3(n_O\pi_L^*)$ state, leading to the delayed fluorescence resulting in the unexpectedly high quantum yield. The slow IC finally leads to the depletion of the $^3(n_O\pi_L^*)$ state to the lowest excited triplet $(\pi_H\pi_L^*)$ state.

We have indeed found features in our results that underscore this explanation. Figure 4 shows that the potential wells of the $^1(\pi_H\pi_L^*)$ and $^3(n_O\pi_L^*)$ cross each other. Besides, the adiabatic minima of the two states lie about 0.03 eV apart, with the triplet minimum lying above the singlet minimum. The energy difference between the adiabatic minimum of the $^1(\pi_H\pi_L^*)$ state and the crossing point of the energy wells is approximately 565 cm^{-1} (at $T = 0$ K), which is only about twice k_BT at room temperature. Hence, ISC crossing between the two states should be feasible at ambient temperature. Similar results have already reinforced the delayed fluorescence for TX in methanol.[7]

Heinz et al. in their work[36] mention an energy barrier for the IC from the $^3(n_O\pi_L^*)$ state to the lower $^3(\pi_H\pi_L^*)$ state causing this channel to be quite slow as compared to the case of X in ethanol. The LIP between the two respective triplet states minima and beyond (see Figure 4), however, shows no such energy barrier. The slow IC between the two triplets should be expected as these states move further apart in water ($\Delta E^{ad} = 0.67$ eV). In their work Heinz et al. have assumed the ΔE_{TT} value for X in water to be the same as that for X in ethanol. Our calculations find this assumption to be misleading, as ΔE_{TT} in water is about 0.3 eV larger than that in methanol, which is

dx.doi.org/10.1021/jp401755j | J. Phys. Chem. A 2013, 117, 3935−3944

comparable to ethanol environment (see Figure 6). Besides, the coupling between the two triplet states should be weak because the nuclear displacement between them is minimal (see Table 1 and section 3.3), indicating a slow IC rate. The temperature dependence of the delayed fluoresence is also clear from the present study: the $^3(n_O\pi_L^*)$ minimum in water lies about 0.03 eV above that of the $^1(\pi_H\pi_L^*)$ state at 0 K, indicating that the process should be an activated one. An alternative IC channel to the lowest triplet may also be via the two multiconfigurational triplets, which also lie in the vicinity of the $^3(n_O\pi_L^*)$ minimum. In the cases discussed above, these states were always unavailable from the $^3(n_O\pi_L^*)$ minimum for IC. However, in the aqueous solution, they have been stabilized so far in energy that one may probably not ignore their role in the depopulation of the triplet $(n_O\pi_L^*)$ state.

4. CONCLUSIONS

A quantum chemical investigation of X in vacuum and various solvents has been carried out. For this purpose, the ground-state minima in all of the cases have been determined and tested for being a true minimum. An examination of the vertical excitation spectra in the cases studied allowed us to come to the conclusion that the blue shift experienced by $(n_O\pi_L^*)$ states is much larger than the corresponding red shifts of the $(\pi\pi^*)$ states as the polarity and proticity of the solvents increase. The relatively large jump in the energy of the $(n_O\pi_L^*)$ states results in a crossing of these and the $(\pi\pi^*)$ states. This, in turn, results in outstanding variations in the photophysical behavior of the chromophore in various media, which has been presented in detail in section 3.3.

Adiabatic minima of the excited states in the singlet and triplet manifold have been found and analyzed to achieve a better understanding of the photophysical behavior of this chromophore. We have presented a detailed discussion of the various photophysical processes occurring (or that may be possbile) for X in vacuum, acetonitrile, methanol, and water. We find that in vacuum an El-Sayed forbidden channel is extremely fast and, hence, becomes a major factor in steering the photophysics. The kinetics in vacuum is best explained by a combination of the branched-sequential kinetics models. As the polarity of the system is increased by taking acetonitrile as the environment of the chromophore, the kinetics changes. The branched model best explains the photophysics in this solvent. By taking methanol as the environment of the chromophore, we have kept the polarity nearly unchanged with respect to acetonitrile but allowed hydrogen bonding to come into play. The energetic shifts are enhanced, and the photophysical processes are best explained by a combination of both branched and sequential models. The extreme polar case including specific bond formation is taken into account by the aqueous solution. The fluorescence is now observable, and the interesting phenomenon of delayed fluorescence via back population of the photoexcited singlet state could occur. The interpretation provided by Heinz et al.[36] for the observed photophysical behavior of xanthone peptide in water is corroborated by our analysis. Because this system, according to the previous authors, is nearly identical in its photophysics to X in water, we can safely assume our theoretical model to be valid.

AUTHOR INFORMATION

Corresponding Author

*E-mail: vidi_shal@yahoo.com.

Notes

The authors declare no competing financial interest.

ACKNOWLEDGMENTS

Financial support by the Deutsche Forschungsgemeinschaft through MA 1051/12-1 is gratefully acknowledged.

REFERENCES

(1) Jockusch, S.; Timpe, H. J.; Schnabel, W.; Turro, N. J. *J. Phys. Chem.* **1997**, *101*, 440−445.
(2) Shan, T.; Ma, Q.; Guo, K.; Liu, J.; Li, W.; Wang, F.; Wu, E. *Curr. Mol. Med.* **2011**, 21902651.
(3) Dahanukar, S. A.; Kulkarni, R. A.; Rege, N. N. *Indian J. Pharm.* **2000**, *32*, 81−118.
(4) Kumar, R.; Kumari, M. *J. Chem. Pharm. Res.* **2011**, *3*, 217−230.
(5) Dzierzbicka, K.; Kolodziejczyk, A. M.; Wysocka-Skrzela, B.; Myśliwski, A.; Sosnowska, D. *J. Med. Chem.* **2001**, *44*, 3606−3615.
(6) Rai-Constapel, V.; Kleinschmidt, M.; Salzmann, S.; Serrano-Andrés, L.; Marian, C. M. *Phys. Chem. Chem. Phys.* **2010**, *12*, 9320−9327.
(7) Rai-Constapel, V.; Salzmann, S.; Marian, C. M. *J. Phys. Chem. A* **2011**, *115*, 8589−8596.
(8) Wöll, D.; Laimgruber, S.; Galetskaya, M.; Smirnova, J.; Pfleiderer, W.; Heinz, B.; Gilch, P.; Steiner, U. E. *J. Am. Chem. Soc.* **2007**, *129*, 12148−12158.
(9) Connors, R. E.; Christian, W. R. *J. Phys. Chem.* **1982**, *86*, 1524−1528.
(10) Pownall, H. J.; Huber, J. R. *J. Am. Chem. Soc.* **1971**, *93*, 6429−6436.
(11) Scaiano, J. C. *J. Am. Chem. Soc.* **1980**, *102*, 7747−7753.
(12) Cavaleri, J. J.; Prater, K.; Bowman, R. M. *Chem. Phys. Lett.* **1996**, *259*, 495−502.
(13) Ley, C.; Morlet-Savary, F.; Fouassier, J. P.; Jacques, P. *J. Photochem. Photobiol., A* **2000**, *137*, 87−92.
(14) Kind, C.; Reiher, M.; Neugebauer, J. *SNF Version 2.2.1: A Program Package for Numerical Frequency Analyses*; Universität Erlangen, 1999−2002.
(15) Salzmann, S.; Marian, C. M. *Photochem. Photobiol. Sci.* **2009**, DOI: 10.1039/b9pp00022d.
(16) Salzmann, S.; Tatchen, J.; Marian, C. M. *J. Photochem. Photobiol., A* **2008**, *198*, 221−231.
(17) Rodriguez-Serrano, A.; Rai-Constapel, M. C. D.; Doerr, M. H. O.; Marian, C. M. *Photochem. Photobiol. Sci.* **2012**, *11*, 1860−1867.
(18) Klamt, A.; Schüürmann, G. *J. Chem. Soc., Perkin Trans. 2* **1993**, *5*, 799−805.
(19) Schäfer, A.; Klamt, A.; Sattel, D.; Lohrenz, J.; Eckert, F. *Phys. Chem. Chem. Phys.* **2000**, *2*, 2187−2193.
(20) Grimme, S.; Waletzke, M. *J. Chem. Phys.* **1999**, *111*, 5645−5656.
(21) Silva-Junior, M. R.; Schreiber, M.; Sauer, S. P. A.; Thiel, W. *J. Chem. Phys.* **2008**, *128*, 104103/1−14.
(22) Marian, C. M.; Gilka, N. *J. Chem. Theory Comput.* **2008**, *4*, 1501−1515.
(23) Tatchen, J. *VIBES*; Universität Düsseldorf: Germany, 2005.
(24) Kleinschmidt, M.; Tatchen, J.; Marian, C. M. *J. Comput. Chem.* **2002**, *23*, 824−833.
(25) Kleinschmidt, M.; Marian, C. M. *Chem. Phys.* **2005**, *311*, 71−79.
(26) Henry, B. R.; Siebrand, W. *J. Chem. Phys.* **1971**, *54*, 1072−1085.
(27) Tatchen, J.; Gilka, N.; Marian, C. M. *Phys. Chem. Chem. Phys.* **2007**, *9*, 5209−5221.
(28) Onuma, S.; Ijima, K. *Acta Crystallogr.* **1990**, *C46*, 1725−1727.
(29) Gales, L.; Damas, A. M. *Curr. Med. Chem.* **2005**, *12*, 2499−2515.
(30) Ohshima, Y.; Fujii, T.; Fujita, T.; Inaba, D.; Baba, M. *J. Phys. Chem. A* **2003**, *107*, 8851−8855.
(31) Ishijima, S.; Higashi, M.; Yamaguchi, H. *J. Phys. Chem.* **1994**, *98*, 10432−10435.
(32) El-Sayed, M. A. *Acc. Chem. Res.* **1968**, *1*, 8−16.
(33) Minaev, B.; Wang, Y.-H.; Wang, C.-K.; Luo, Y.; Ågren, H. *Spectrochim. Acta, Part A* **2006**, *65*, 308−323.

(34) Englman, R.; Jortner, J. *Mol. Phys.* **1970**, *18*, 145−164.
(35) Satzger, H.; Schmidt, B.; Root, C.; Zinth, W.; Fierz, B.; Krieger, F.; Kiefhaber, T.; Gilch, P. *J. Phys. Chem. A* **2004**, *108*, 10072−10079.
(36) Heinz, B.; Schmidt, B.; Root, C.; Satzger, H.; Milota, F.; Fierz, B.; Kiefhaber, T.; Zinth, W.; Gilch, P. *Phys. Chem. Chem. Phys.* **2006**, *8*, 3432−3439.